# Chemical Science

Accepted Manuscript


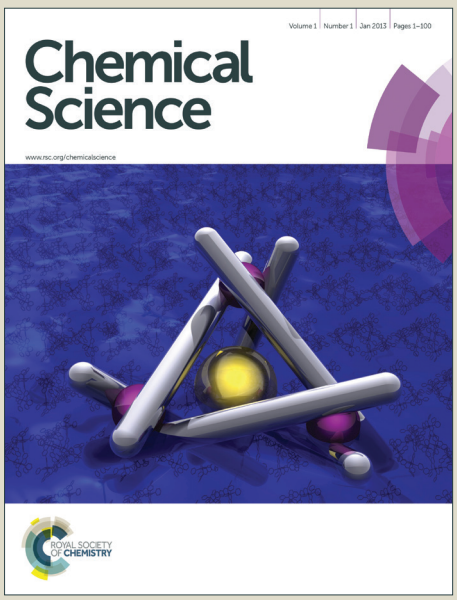





ROYAL SOCIETY OF CHEMISTRY

www.rsc.org/chemicalscience

Journal Name

RSCPublishing

ARTICLE

# A Precision Structural Model for Fullerenols

Cite this: DOI: 10.1039/xoxxoooooox

Zhenzhen Wang,[a,b] Xueling Chang,[a] Zhanghui Lu,[b] Min Gu,[c] Yuliang Zhao,[*,a] and Xingfa Gao[*,a]

Received ooth January 2012,
Accepted ooth January 2012

DOI: 10.1039/xoxxoooooox

www.rsc.org/

Fullerenol is one of the main precursors of fullerene-based materials, which is promising for various biological applications because of its unusual biocompatibility and biofunctionality. However, the functional groups, acidity and reducibility, which substantialize the applications of fullerenols, remain open questions. Using density functional theory calculations, we investigated reaction mechanisms underlying the acidity and reducibility of $C_{60}$ fullerenols. On the basis of theoretical insights combined with synthesis, IR and NMR structural characterization of $^{13}C$-labeled $C_{60}$ fullerenols, we identified the functional groups and developed and verified a structural model for $C_{60}$ fullerenols. The results show a strong dependence of acidity and reducibility on the hydroxyl distributions of fullerenols. Fullerenols with stable π-electron configurations on $C_{60}$ cores, in which no double bonds have to be placed in conjugated pentagonal rings when drawing their Kekulé structures, have low acidities and reducibilities. Contrarily, fullerenols with unstable π-electron configurations have high acidities and reducibilities. For fullerenols with different hydroxyl distributions, the calculated acid dissociation constants range from –17.55 to 15.21, and the calculated redox potentials range from –0.87 to 1.32 V. Hydroxyls with high acidities and reducibilities unlikely survive in fullerenols synthesized using alkali, oxidizing conditions. Instead, they exist as the corresponding conjugate bases or oxidized products. This structural prediction agrees with our NMR results and the previous experiments. The proposed structural model is able to interpret the main IR and NMR spectroscopic and electronically paramagnetic properties of $C_{60}$ fullerenols without the disadvantages of the previous models.

## Introduction

Fullerene, which consists entirely of hydrophobic $sp^2$ carbon atoms, hardly dissolves in water. Increasing its solubility in water is usually necessary before applying fullerenes in aqueous conditions, *e.g.*, biological systems. To date, the most common approach to produce water-soluble fullerenes is through hydroxylation reactions, *i.e.*, reactions with oxidizing agents that transfer hydrophilic hydroxyl (OH) groups onto fullerene surfaces. The obtained fullerene derivatives, namely fullerenols, have solubility in water scaling with the numbers of added OH.

Recent studies have demonstrated that fullerenols synthesized in the oxygenated, aqueous NaOH solution have intriguing biomedical effects such as antioxidant, antitumor and antimetastatic activities.[1-7] Because fullerenols thus obtained are amorphous mixtures, developing explicit structural models for them is urgent before studying the mechanisms underlying their biofunctionalities and before designing new fullerene-based nanodrugs for improved biomedical effects. Especially, such models are prerequisites to take advantage of the various all-atom simulation approaches, which are indispensable to study the structure-activity relationships for fullerenols at atomistic levels.

The lack of explicit structural models also makes it difficult to understand the fundamental properties of fullerenols. $C_{60}$ fullerenols has been experimentally characterized to be a stable radical anion, in which units of cyclopentadienyl anion are proposed to exist, responsible for the observed radical anion property.[8] However, because a cyclopentadienyl anion has six π-electrons and is aromatic without radical electrons, it cannot substantialize the radical nature. Hitherto, infrared (IR) spectroscopy is among the few approaches revealing structural information at atomistic levels for $C_{60}$ fullerenols. According to the IR results, $C_{60}$ fullerenols had characteristic adsorptions at 1080, 1370, 1620 and 3400 $cm^{-1}$, which were assigned to $\nu$C–O, $\delta_S$C–O–H, $\nu$C=C and $\nu$O–H adsorptions.[9-12] This assignment was consistently made by all research groups, evidencing the presence of OH in $C_{60}$ fullerenols. Besides, an absorption peak at 1720 $cm^{-1}$ was observed for fullerenols synthesized using alkali, oxidizing conditions.[8, 10, 13] Chiang *et al.* for the first time found this absorption disappeared after the sample was treated with NaOH and reappeared after it was treated with HCl. Although this peak was invariably assigned to $\nu$C=O, the explanation of its origin and pH-dependent transformation mechanism is an uncertainty. Chiang *et al.* proposed two possible mechanisms: the tautomerization between a hemiacetal and a hydroxyl-ketone structure and the rearrangement between

a *vic*-diol to a ketone structure. They concluded that hemiacetal units existed in $C_{60}$ fullerenols, responsible for the observation.[12] Because the overall reaction of any tautomerization is independent from $H^+$ or $OH^-$, they cannot substantialize the pH-dependency of the transformations. Alternatively, Kokubo *et al.* reported the possible existence of carboxyl groups due to an over oxidation of $C_{60}$. They suggested attributing the disappearance of the peak at 1720 $cm^{-1}$ in alkali conditions to the red shift of carboxylic C=O while forming carboxyl anion.[9] However, no further experiments support the existence of carboxyl in $C_{60}$ fullerenols.

Here, to identify the functional groups of $C_{60}$ fullerenols survivable in alkali, oxidizing conditions, we have investigated the reaction mechanisms underlying the acidity and reducibility of $C_{60}$ fullerenols using density functional theory (DFT) calculations. We have also synthesized $^{13}C$-labeled $C_{60}$ fullerenols and performed nuclear magnetic resonance (NMR) and IR characterizations. On the basis of theoretical insights combined with experimental characterizations, we have developed and verified a structural model for $C_{60}$ fullerenols. The model well substantializes the fundamental properties observed for $C_{60}$ fullerenols so far and provides a basis for the study of the structure-activity relationships in the future.

## Results and Discussion

### Acidity

The acid dissociation reactions were studied for three simple but typical $C_{60}$ fullerenols, **1a**, **1b** and **1c** (Figure 1). **1a** and **1b** are *vic*-diols with OH groups located at the 6,6- and 5,6-ring junctions of $C_{60}$ (6,6- and 5,6-*vic*-diols). Diol **1c** has the two OH located on the opposite poles of $C_{60}$ core. **1d** is the intermediate connecting **1a** and **1b** (group 1). The rest of the structures in Figure 1 are those involved in the acid dissociation reactions or the corresponding structural isomers. **2f** and **2g** are formally the conjugate bases of **2a** and **2b**, respectively; **2c**–**2j** are structural isomers of **2f** and **2g** (group 2). **3a**–**3f** are ketone, ether or epoxide structures, which are isomers of the diols with both protons detached (group 3). **4a**–**4d** are mono-oxygenated $C_{60}$ (group 4). Because structures in each of the four groups are isomers, relative thermodynamic stabilities can be easily obtained by comparing the calculated Gibbs free energies. The relative Gibbs free energies ($G_{rel}$) of these structures in gas phase and water are listed in Table S1 of supporting formation. Reactions connecting these structures and the calculated Gibbs free energy changes and barriers are given in Table 1 if the barriers exist.

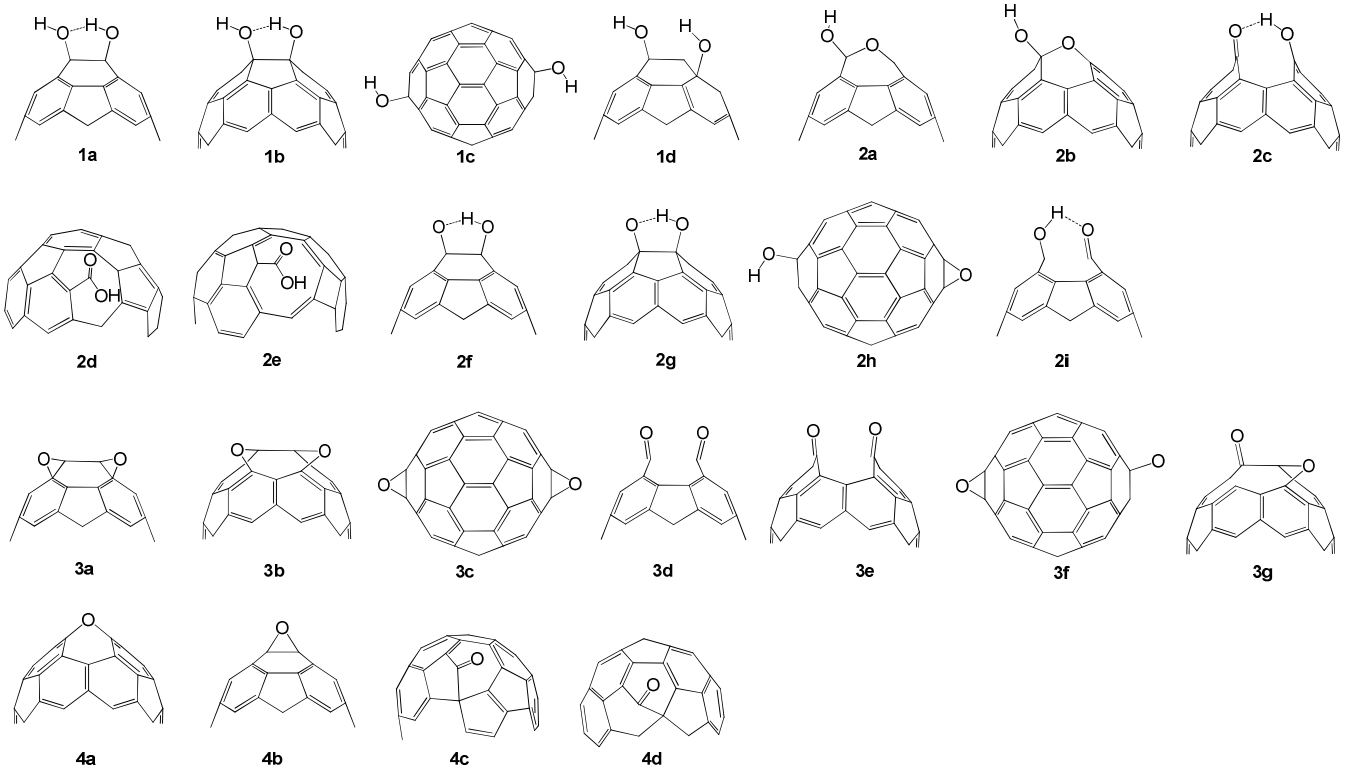


***Figure1.*** Structures of $C_{60}$ diols, the conjugate bases, oxidized structures and other derivatives.

According to Table S1 of supporting formation, *vic*-diol **1a** is more thermodynamically stable than **1b** by ~15 kcal/mol in gas phase and water, which is consistent with the previous reports that 6,6-adduct of $C_{60}$ has a lower energy than the corresponding 5,6-adduct for 1,2-addition reactions.[14] The preference of 6,6-adduct has been ascribed to the shorter bond length and thus larger reactivity of 6,6-bond.[15-17] **1c** (triplet is the lowest energy state) has a much higher energy than **1a** and **1b**. According to Table 1, **1b** can transform to **1a** via reactions 1 and 2. The rate-determining step of this transformation is reaction 1, *i.e.*, the conversion of **1b** to intermediate **1d**. This step has an energy barrier of 40.2 kcal/mol. The barrier implies that the transformation between **1a** and **1b** is kinetically unfavorable. Similarly, the mutual conversion among **1a**, **1b** and **1c** is kinetically unfavorable. Hence, we investigated the structures of conjugate bases for **1a**, **1b** and **1c** separately.



 

According to Table 1, **1a** (**1b**, **1c**) readily reacts with $OH^-$, giving a $H_2O$ molecule and the conjugate base $\mathbf{2f}^-$ ($\mathbf{2g}^-$, $\mathbf{2h}^-$).

***Table 1.*** Gibbs Free-energies Barriers ($G^{\neq}$) and Changes ($\Delta G$) (kcal/mol) Calculated in Gas Phase and Water (in Parentheses)

| reactions | $G^{\neq}$ | $\Delta G$ |
|---|---|---|
| (1) **1b** = **1d** | 40.2 (41.4) | 27.9 (25.4) |
| (2) **1d** = **1a** | 11.7 (14.3) | –44.4 (–41.1) |
| (3) **1a** + $OH^-$ = $\mathbf{2f}^-$ + $H_2O$ | | –105.6 (–33.0) |
| (4) $\mathbf{2f}^-$ = $\mathbf{2a}^-$ | 48.7 (57.9) | –0.6 (9.6) |
| (5) **1b** + $OH^-$ = $\mathbf{2g}^-$ + $H_2O$ | | –102.9 (–31.2) |
| (6) $\mathbf{2g}^-$ = $\mathbf{2c}^-$ | 1.9 (6.9) | –3.8 (7.0) |
| (7) $\mathbf{2c}^-$ = $\mathbf{2b}^-$ | 11.7 (10.6) | –25.1 (–24.3) |
| (8) **1c** + $OH^-$ = $\mathbf{2h}^-$ + $H_2O$ | | –137.8 (–51.8) |
| (9) $\mathbf{2b}^-$ + $OH^-$ = $\mathbf{3e}^{2-}$ + $H_2O$ | | –42.3 (–26.3) |
| (10) $\mathbf{3e}^{2-}$ = $\mathbf{3g}^{2-}$ | 69.5 (69.3) | 44.7 (32.5) |
| (11) $\mathbf{3g}^{2-}$ = $\mathbf{3b}^{2-}$ | 2.1 (9.7) | –33.6 (–15.1) |
| (12) **2f** = **2i** | 7.8 (8.1) | 1.2 (2.9) |
| (13) **2i** = **2a** | 20.2 (19.0) | –18.8 (–18.5) |
| (14) **2g** = **2c** | 3.8 (3.9) | –11.0 (–7.1) |
| (15) **2c** = **2b** | 11.0 (11.3) | –25.7 (–23.6) |

***Table 2.*** Calculated Acid Dissociation Constants ($pK_a$) for $C_{60}$ Fullerenols[a]

| Acid | $pK_{a1}$ | acid | $pK_{a2}$ |
|---|---|---|---|
| acetic acid | 4.76 | | |
| formic acid | 1.46 | | |
| phenol | 9.22 | | |
| benzoic acid | 3.80 | | |
| **1a** (= $\mathbf{2f}^-$ + $H^+$) | 6.31[a] | $\mathbf{2f}^-$(= $\mathbf{3d}^{2-}$ + $H^+$) | 23.46 |
| **1b** (= $\mathbf{2b}^-$ + $H^+$) | –4.94[a] | $\mathbf{2b}^-$ (= $\mathbf{3e}^{2-}$ + $H^+$) | 11.13 |
| **1c** (= $\mathbf{2h}^-$ + $H^+$) | –3.72[a] | $\mathbf{2h}^-$ (= $\mathbf{3f}^{2-}$ + $H^+$) | 21.70 |
| **6a** (= $\mathbf{8a}^-$ + $H^+$) | 13.32[a] | | |
| **6b** (= $\mathbf{8b}^-$ + $H^+$) | 15.21[a] | | |
| **7** (= $\mathbf{9}^-$ + $H^+$) | –17.55[a] | | |

[a]The experimental $pK_a$ for acetic acid, formic acid, phenol and benzoic acid are 4.76, 3.77, 9.96 and 4.20, respectively.

This reaction has an exothermicity of –33.0 (–31.2, –51.8) kcal/mol in water (see reactions 3, 5 or 8 of Table 1). $\mathbf{2g}^-$ can further transform to hemiacetal structure $\mathbf{2b}^-$ via reactions 6 and 7 (Table 1) and intermediate $\mathbf{2c}^-$. In $\mathbf{2b}^-$, the deprotonation induced the formation of an open-bonded ether, which releases the strain energy of the $C_{60}$ core. The overall reaction from $\mathbf{2g}^-$ to $\mathbf{2b}^-$ is exothermic by –17.3 (*i.e.*, –24.3 + 7.0) kcal/mol and the rate-determining step has only a low activation barrier of ~10 kcal/mol. Therefore, hemiacetal structure $\mathbf{2b}^-$ is the dominant conjugate base of **1b**. In contrast, the conversion from $\mathbf{2f}^-$ to the corresponding hemiacetal $\mathbf{2a}^-$ is endothermic in water and has a high energy barrier more than 48 kcal/mol (see reaction 4 of Table 1). In $\mathbf{2f}^-$, the two O atoms of the pristine OH groups share one H atom. The energy barrier for the H shifting from one O to the other is negligibly small, suggesting the H readily migrates. Consequently, the H-shared structure $\mathbf{2f}^-$ is the dominant conjugate base of **1a**. Such different preference for the structures of conjugate bases agrees with the previous experimental results that 6,6-bond of $C_{60}$ readily yields closed-bond adducts and 5,6-bond of $C_{60}$ yields open-bond adducts for 1,2-cycloaddition reactions.[18] $\mathbf{2h}^-$ is the dominant conjugate base of **1c**. In $\mathbf{2h}^-$, the deprotonated O forms another covalent bond with $C_{60}$ to give an epoxide. In each of **1a**, **1b** and **1d**, the total number of charges on the OH is about 0.3 $e^-$ (Figure S1 of supporting formation). This means each $C_{60}$ cage has a charge of 0.3 $e^+$. As for $\mathbf{2f}^-$, the charge of 1 $e^-$ is nearly entirely distributed on the two oxygen atoms, leaving $C_{60}$ cage electrically neutral. In $\mathbf{2b}^-$ and $\mathbf{2h}^-$, the $C_{60}$ cages have negative charges of 0.6 $e^-$ and –0.5 $e^-$, respectively.

The subsequent acid dissociation reactions for $\mathbf{2f}^-$, $\mathbf{2b}^-$ and $\mathbf{2h}^-$ were also studied. The deprotonation of these species gives $\mathbf{3d}^{2-}$, $\mathbf{3e}^{2-}$ and $\mathbf{3f}^{2-}$, respectively. Structural isomers such as $\mathbf{3a}^{2-}$, $\mathbf{3b}^{2-}$, $\mathbf{3c}^{2-}$ and $\mathbf{3g}^{2-}$ exist but have higher energies than $\mathbf{3d}^{2-}$ and $\mathbf{3e}^{2-}$. For example, $\mathbf{3b}^{2-}$ is energetically higher than $\mathbf{3e}^{2-}$ by 17.4 kcal/mol in water (Table S1). Although they are connected via reactions 10 and 11 (Table 1), the conversion between $\mathbf{3b}^{2-}$ and $\mathbf{3e}^{2-}$ has a high energy barrier of 69.5 kcal/mol. Therefore, $\mathbf{3d}^{2-}$, $\mathbf{3e}^{2-}$ and $\mathbf{3f}^{2-}$ are the dominant conjugate bases for $\mathbf{2f}^-$, $\mathbf{2b}^-$ and $\mathbf{2h}^-$, respectively.

To better understand the acidities of $C_{60}$ fullerenols, acid dissociation constants $pK_{a1}$ and $pK_{a2}$ for diols **1a**, **1b** and **1c** were calculated (Table 2). The $pK_{a1}$ are 6.31, –4.94 and –3.72 and the $pK_{a2}$ are 23.46, 11.13 and 21.70, respectively. For comparison, the $pK_a$ values for acetic acid, benzoic acid and phenol are also given in Table 2, which are 4.76, 4.20 and 9.96, respectively.[19] The results show that $C_{60}$ diols have a strong dependence of acidities on OH distributions. **1a** has a low acidity, whose $pK_a$ value is between those of acetic acid and phenol. However, **1b** and **1c** have much stronger acidities, with $pK_a$ values markedly lower than that of benzoic acid. According to Table S1, the strong acidities of **1b** and **1c** can be ascribed to their large thermodynamic instability compared with **1a**. Taking **1a** and **1b** as an example, although the conjugate bases $\mathbf{2f}^-$ and $\mathbf{2b}^-$ have nearly equal relative energies, the energy of **1b** is higher than that of **1a** by 15 kcal/mol.

Here, we will use a more straightforward way to interpret the position dependent acidities of diols. Reportedly, the stable π-electron configuration of $C_{60}$ is that all the sixty π-electrons form double bonds at the 6,6-ring junctions. The placement of each double bond in a conjugated pentagonal ring causes an energy increase of 8.5 kcal/mol.[20, 21] Namely, all double bonds are outside of the pentagonal rings. This π-configuration is consistent with the polyolefin-like chemical properties established for $C_{60}$. As shown in Figure 1, **1a** and its conjugate base $\mathbf{2f}^-$ already have stable π-configurations with all double bonds at 6,6-ring junctions. In contrast, **1b** has an unstable π-configuration, in which two double bonds (*i.e.*, bonds i and ii, see **1b** of Figure 1) have to be placed at pentagonal edges when drawing its Kekulé structure. However, its conjugate base $\mathbf{2b}^-$ has a stable π-configuration without pentagonal double bonds. Similarly, **1c** has 8 double bonds at pentagonal edges but the corresponding conjugate base $\mathbf{2h}^-$ has no such double bonds (Figure S2 of supporting formation). Therefore, the acid dissociation reaction from **1b** to $\mathbf{2b}^-$ and that from **1c** to $\mathbf{2h}^-$ stabilize the π-electron configurations while that from **1a** to $\mathbf{2f}^-$ does not. This profoundly interprets the higher acidities of **1b** and **1c** than that of **1a**.

Journal Name RSCPublishing

ARTICLE

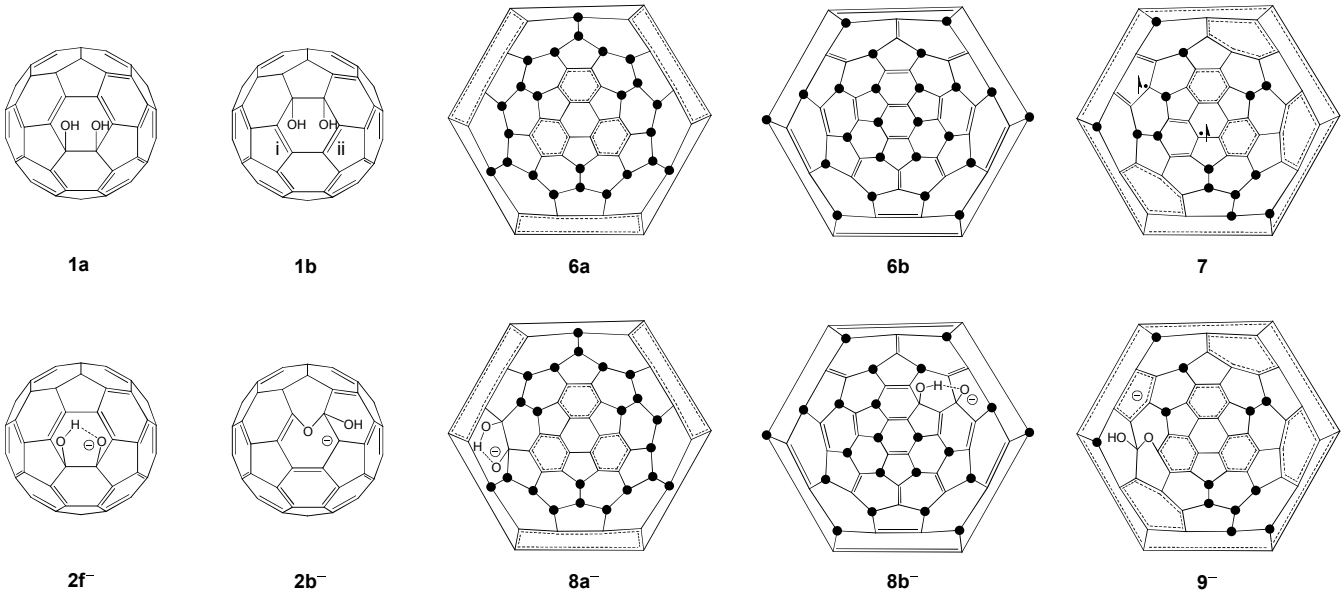


***Figure 2.*** Skeletal structures and π-electron configurations for $C_{60}$ fullerenols (top) and the corresponding conjugated bases (bottom).

The strong dependence of acidities on π-electron configurations found for diols also holds for fullerenols with multiple hydroxyls. **6a** and **6b** are two $C_{60}(OH)_{24}$ isomers and **7** is a $C_{60}(OH)_{14}$ isomer (Figure 2). All π-electrons in **6a** form aromatic benzenoid rings linked by single bonds and all π-electrons in **6b** form double bonds isolated by $sp^3$ carbons. Therefore, both **6a** and **6b** have stable π-configurations and are expected to have weak acidities. However, the π-electrons in **7** form four pentagonal double bonds and two radical electrons in addition to benzenoid rings (Figure 2). In the corresponding conjugate base **9**$^-$, all π-electrons are stabilized in six-π-electron aromatic rings linked by single bonds. Therefore, **7** is expected to have a strong acidity. Indeed, the p$K_a$ values calculated for **6a**, **6b** and **7** are 13.32, 15.21 and –17.55, respectively (Table 2). These results suggest that the acidities of fullerenols reflect the extents of π-electron stabilizations accompanying the acid dissociation reactions. A strong acidity is a consequence of a large π-electron stabilization and vice versa.

**Reducibility**

The donations of one H· from **1a**, **1b** and **1c** yield **2a**$^·$, **2b**$^·$ and **2h**$^·$, and the subsequent donations of the other H· yield **3d**, **3b** and **3c** as the lowest-energy products, respectively (for the formation pathways of **2a** and **2b**, see reactions 12-15 of Table 1). The oxidized product of **1a** (*i.e.*, **2a**$^·$) has an open-bonded hemiacetal structure, which is different from the conjugate base of **1a** (*i.e.*, **2f**$^-$) with a H-shared structure. This is because O has a strong ability to accommodate extra electrons, rending O in an anionic state as in **2f**$^-$. However, O has a weak ability to accommodate radical electrons. Therefore, it prefers the hemiacetal structure in oxidation reactions, rending the radical electron to be located on the $C_{60}$ core as in **2a**$^·$.

***Table 3.*** Calculated Redox Potentials ($\varepsilon$) for $C_{60}$ Fullerenols[a]

| redox couple | $\varepsilon$ (V) | redox couple | $\varepsilon$ (V) |
|---|---|---|---|
| GSSG/GSH | –0.24 | | |
| **2a**$^·$/**1a** | 0.53 | **3d**/**2a**$^·$ | –0.28 |
| **2b**$^·$/**1b** | –0.39 | **3b**/**2b**$^·$ | –0.18 |
| **2h**$^·$/**1c** | –0.29 | **3c**/**2h**$^·$ | –0.20 |
| **8a**$^·$/**6a** | 0.18 | **8b**$^·$/**6b** | 1.32 |
| **9**$^·$/**7** | –0.87 | | |

[a]The experimental $\varepsilon$ for GSSG/GSH is –0.23 V.

Table 3 lists the redox potentials ($\varepsilon$) calculated for the redox couples, including those of **6a**, **6b** and **7**. For comparison, $\varepsilon$ for an important biological antioxidant, glutathione (GSH) is also given. The redox couples **2a**$^·$/**1a**, **8a**$^·$/**6a** and **8b**$^·$/**6b** have positive $\varepsilon$ values (0.53, 0.18 and 1.32 V), which are more positive than that of GSSG/GSH. This suggests the tendency of GSH to donate electrons (*i.e.*, H) to **2a**$^·$, **8a**$^·$ and **8b**$^·$ to form **1a**, **6a** and **6b**, respectively. In contrast, all the other couples have negative $\varepsilon$ values. The values of $\varepsilon_{\mathbf{2b/1b}}$, $\varepsilon_{\mathbf{3d/2a}}$, $\varepsilon_{\mathbf{2h/1c}}$ and $\varepsilon_{\mathbf{9/7}}$ are even more negative than that of GSSG/GSH, indicating the tendency of **1b**, **1c**, **2a**$^·$ and **7** to donate electrons to GSSG to form GSH. Namely, the reducibilities of **1a**, **6a** and **6b** are lower than that of GSH. However, fullerenols **1b**, **1c** and **7** have stronger reducibilities than GSH. The ordering of $\varepsilon$ values is close to that of p$K_a$ values for these fullerenols. Therefore, similar to acidities, the reducibilities of fullerenols also reflect the extents of π-electron stabilizations accompanying the H·-donation reactions. A strong reducibility is a consequence of a large π-electron stabilization and vice versa.

To better understand the dependence of acidity and reducibility on hydroxyl distribution of $C_{60}$ fullerenols, we systematically investigated the acidities and reducibilities for 23 symmetrically unique $C_{60}$ diol structures, which are denoted as **1** through **23** here after (Figure 3a). According to our calculated results, the ground states for **1**-**7** and **10**-**12** are closed-shell singlets; those for **8**, **9**, **13** and **23** are open-shell singlets; those for **14**-**22** are triplets (Table S2 of supporting formation). This is consistent with the result of 2H-addition to $C_{60}$[20]. All these diols donate $H^+$ through mechanisms (i), (ii) and (iii) as shown in Figure 3b. All of them prefer mechanism iii, except for 6,6-*vic*-diol (**1**) and 5,6-*vic*-diol (**4**), which prefer mechanisms (i) and (ii), respectively. The acidities of these diols have a surprisingly large dependence on hydroxyl distributions. Figure 3c plots the acid dissociation constants ($pK_a$) calculated for these diols. Diols **1**, **2** and **3** have only weak acidities, with $pK_a$ larger than six. In contrast, all the other diols have $pK_a$ less than three, having much stronger acidities. Among them, 5,6-*vic*-diol has the strongest acidity with $pK_a$ = −4.9. For reducibility, these diols will donate H· via mechanisms (iv) and (v) as shown in Figure 3b. All diols prefer mechanism (v), except for 6,6 and 5,6-*vic*-diols, which prefer mechanism (iv). Figure 3c also plots the calculated redox potentials ($\varepsilon$). The reducibility ($\varepsilon$) is nearly in direct proportional to acidity ($pK_a$). These results suggest valuable structural information for $C_{60}$ fullerenols. For diols, only **1**, **2** and **3** are possible to survive in the alkali, oxidizing synthetic conditions because of their weak acidities and weak reducibility. Contrarily, the other diols will exist as the corresponding conjugated bases or oxidized structures because of their high acidity and reducibility. Combined with the result of relative Gibbs free energies (insert of Figure 3c), 6,6-*vic*-diol and 5,6-hemiactal (*i.e.*, oxidized radical or conjugated base of 5,6-*vic*-diol) will be the most viable structures in $C_{60}$ fullerenols. This agrees with the experimental results that fullerenols synthesized in alkali, oxidizing conditions were stable alkali salts and had paramagnetic characters.[8, 9] Besides, open-bonded ether structures will also prevail as the corresponding conjugate bases or oxidized radicals of other diols. Indeed, the existence of these structural units has been unambiguously identified in $C_{60}$ fullerenols or their derivatives synthesized using the stepwise methods by Gan and coworkers,[15, 22, 23] supporting the high viability of these structures.

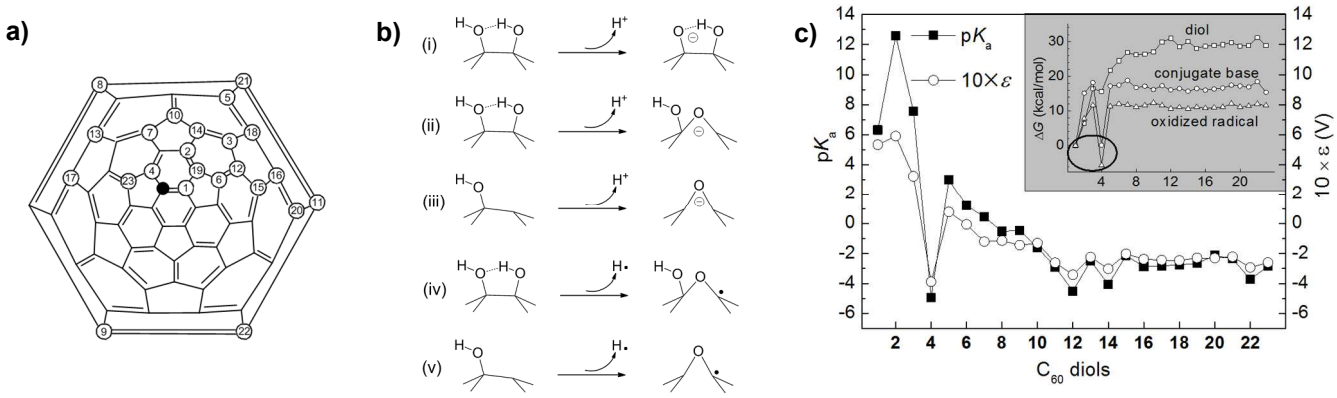


***Figure 3.*** The development and verification of a structural model for fullerenols: (a) a schematic structure showing hydroxyl positions for the 23 $C_{60}$ diols, where the filled circle represents the position of the first hydroxyl and each circled number represents that of the second hydroxyl; (b) $H^+$-donation (*i.e.*, acid dissociation) mechanisms (i-iii) and H·-donation (*i.e.*, oxidation) mechanisms (iv-vi) of $C_{60}$ diols; (c) calculated $pK_a$ and $\varepsilon$ for the 23 $C_{60}$ diols, where the insert shows the relative Gibbs free energies for the diols, the corresponding conjugated bases and oxidized radicals, with the lowest-energy structures in the black circle.

**Structural Model**

To verify whether these structural units exist in $C_{60}$ fullerenols prepared using alkali, oxidizing conditions and to investigate the possible existence of other chemical groups, we synthesized $^{13}C$-labeled $C_{60}$ fullerenols and characterized their structures using the IR. As shown in Figure 4a, the fullerenols has characteristic adsorptions at 1080, 1369, 1593 and 3401 $cm^{-1}$, which can be assigned to $\nu$C–O, $\delta_S$C–O–H, $\nu$C=C and $\nu$O–H adsorptions. This suggests the formation of OH groups on the $C_{60}$ cage. After the sample was treated with HCl, a new absorption at 1720 $cm^{-1}$ appeared (Figure 4b) and this adsorption disappeared again after the sample was recovered with NaOH treatment (Figure 4c). This is consistent with the result of Chiang and co-workers,[12] indicating the pH-dependent reversible formation of carbonyls in the fullerenols. Because the intensities of other adsorption peaks in Figure 4 also dramatically change, the pH alteration may also induce the rearrangement of other chemical groups in the fullerenols.

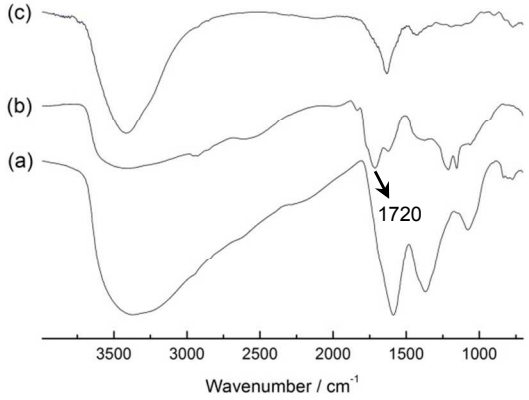


***Figure 4.*** IR spectra of the $C_{60}$ fullerenol (a), solid precipitates from the reaction of the fullerenols with HCl at 80℃ (b), recovered fullerenols from the treatment of the solid with NaOH (c).

Figure 5 shows the NMR spectra. Compared with the previous NMR characterizations,[15, 23, 24] $^{13}$C-labeled samples we used here allowed to obtain NMR spectra with a higher resolution and thus to perform a more detailed structural characterization. As shown in Figure 5a, the broad resonance features at 76.8 and 136.3 ppm can be assigned to the hydroxylated sp$^3$-carbons (*e.g.*, $C_a$ of Figure 6a) and unreacted sp$^2$-carbons (*e.g.*, $C_b$), respectively. This is comparable to our calculated chemical shifts for the hydroxylated sp$^3$-carbons (83.7-61.2 ppm) and unreacted sp$^2$-carbons (148.7-117 ppm) (Table S3 of supporting information). The intensive resonance at 175.6 ppm and the weak resonance at 104.6 ppm can be assigned to the ether sp$^2$-carbons (*e.g.*, $C_c$) and the hemiacetal's sp$^3$-carbons (*e.g.*, $C_d$), respectively. These resonance peaks are consistent with those reported by Chiang and corkers, supporting the presence of OH and hemiacetal groups in $C_{60}$

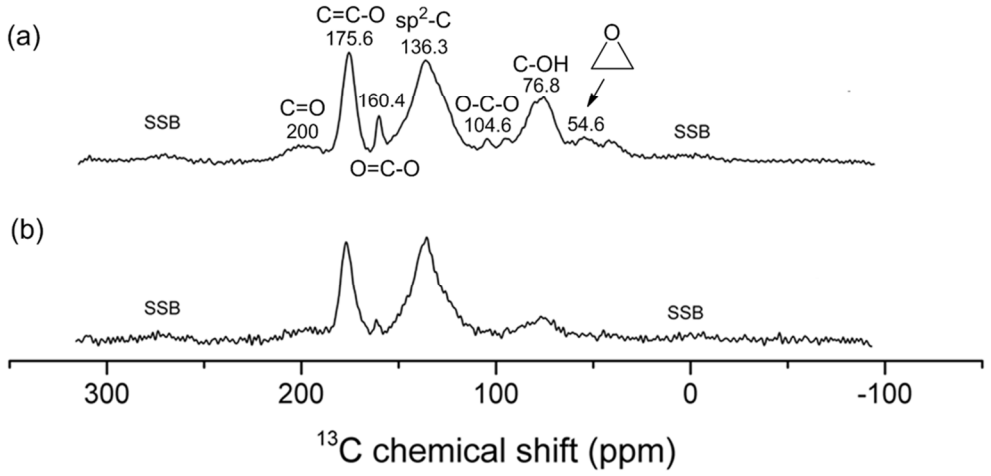


***Figure 5.*** $^{13}$C NMR spectra of $^{13}$C-labeled $C_{60}$ fullerenols; SSB indicates sideband. (a) $^1$H-$^{13}$C CP spectra at contact times of 2 ms; (b) $^{13}$C MAS NMR spectrum of $C_{60}$ fullerenols.

fullerenols.[12] Because the ether sp$^2$-carbons (175.6 ppm) are much larger in amount than the hemiacetal's sp$^3$-carbons (104.6 ppm), ether groups like that in **4a** must also exist, contributing to the majority of the resonance peak at 175.6 ppm. Besides, the weak peaks at 54.6, 160.4 and 200 ppm can be assigned to epoxide, carboxyl and ketone groups, respectively. These assignments agree with those of graphene oxide, in which the NMR resonance peaks at 60, 70, 101, 133, 167 and 191 ppm were assigned to epoxides, hydroxyls, lactols, sp$^2$-carbons, carboxyls and ketones, respectively.[25-29] The abundance of ether structures in fullerenols is in contrast to their absence in graphene oxides. This is because the formation of open-bonded ethers relieves the non-planar strain of $C_{60}$ cages and is thus preferred in fullerenols, but this will not occur for planar, strain-free graphene.

With these structural insights, we developed a model to explain the main structural and electronic properties of $C_{60}$ fullerenols experimentally observed so far. Briefly, the model was constructed by adding hydroxyls (or in the forms of conjugate base and oxidized product), epoxides, ethers, hemiacetals and carboxyls at appropriate positions of the $C_{60}$ cage, leaving the unreacted sp$^2$ carbons to form single-bond-linked aromatic rings as many as possible, because according to the known stability rule for conjugated carbon materials, aromatic rings linked by single bonds are chemically stable with high HOMO-LUMO energy gaps.[30-32] Figure 6a shows such a model as an example. The model has a molecular formula of $C_{60}O_{19}H_{11}^{\bullet 3-}$, which is close to those determined by experiments, *i.e.*, $C_{60}O_xH_y^{\bullet n-}$ ($n$ = 2-3, $x$ = 19-24, $y$ = 12-15).[8] As shown in Figure 6a, the model consists of nine OH, two hemiacetals, two ethers, one epoxide and one carboxyl groups. The unreacted sp$^2$-carbons form aromatic rings linked by single bonds, which will be chemically stable according to the stability rule.[30-32] The deprotonation of the two hemiacetal and

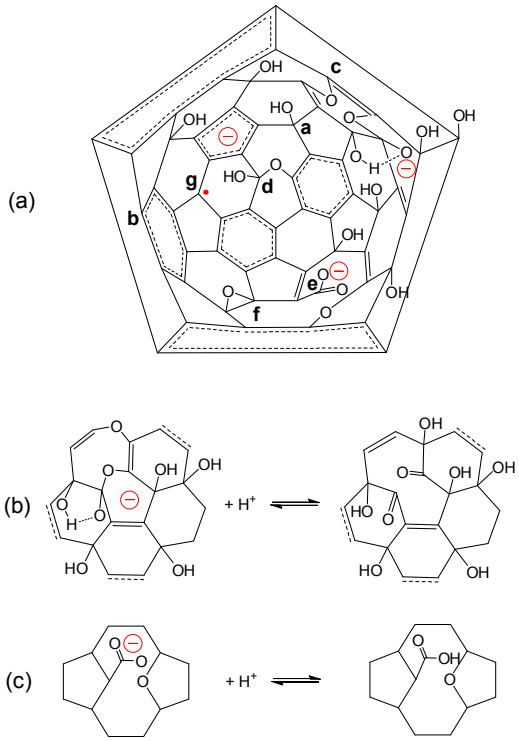


***Figure 6.*** A structural model for $C_{60}$ fullerenols (a) and reactions of partial structures in the model to interpret the pH-dependent transformations of C=O (b, c).

one carboxyl groups renders the model to be a trivalent anion. This agrees with that fullerenols readily form stable salts with alkali metals.[8, 33] The model also has a free radical electron at

$C_g$, the intersection of the three aromatic rings. With the structure similar to that of triphenylmethyl radical, the first-ever radical described in organic chemistry, the radical electron in the model will be pretty stable. Therefore, this model for the first time substantializes the stable anionic radical nature of fullerenols, avoiding the disadvantage of cyclopentadienyl anion model, which fails to account for the radical character.[8] The radical electron in fullerenols is likely from the oxidation of an OH group via mechanism (iv) or (v) (Figure 3b).

The model contains no ketone structures in anionic state, which agrees with the experimental results that no IR adsorptions at about 1720 $cm^{-1}$ were observed for $C_{60}$ fullerenols. However, ketone structures can be formed by reacting with protons (Figure 6b) and can be converted back through the reverse reactions with bases. This agrees with that IR adsorptions at 1720 $cm^{-1}$ appeared after the fullerenols were treated with acids and disappeared after they were treated with bases. The partial structure of Figure 6b has already been experimentally synthesized,[28] the favourable deprotonation reaction of which was indeed calculated to be that of Figure 6b (Figure S3 of supporting information). This supports the introduction of the partial structure of Figure 6b into the model. Because deprotonated carboxyl does not have IR adsorptions at 1720 $cm^{-1}$ but carboxyl does,[9] the reaction of Figure 6c can also explain the pH-dependent IR adsorptions. Therefore, the model of Figure 6a profoundly explains the main IR and NMR spectroscopic and electronically paramagnetic properties of $C_{60}$ fullerenols without the shortcomings of the previous models.[8, 10, 12]

## Conclusion

The acidity of $C_{60}$ fullerenols mainly originates from the $H^+$ donation mechanisms of (i), (ii) or (iii) (Figure 3b), and the reducibility mainly from the H donation mechanisms of (iv) or (v) (Figure 3b). Both acidity and reducibility reflect the extents of stabilization of $C_{60}$-cores' π-electron configurations accompanying the $H^+$ and H· donations. A high acidity and reducibility of fullerenols is a consequence of a large π-electron stabilization effect associated with the $H^+$ and H· donation reactions, respectively, and vice versa. Briefly, fullerenols with stable π-electron configurations of $C_{60}$ cores, in which no double bonds have to be placed in conjugated pentagonal rings when drawing their Kekulé structures, have a low acidity and reducibility. Contrarily, fullerenols with unstable π-electron configurations have a high acidity and reducibility provided that the $H^+$ and H· donation reactions stabilize the π-configurations, respectively. This renders $C_{60}$ fullerenols a strong dependence of acidity and reducibility on hydroxyl distributions. The calculated acid dissociation constants $pK_{a1}$ range from –17.55 to 15.21, and the redox potentials range $\varepsilon$ from –0.87 to 1.32 V.

The above dependence of acidity and reducibility on hydroxyl distributions provides useful insights into the local structures of fullerenols. In terms of $C_{60}$ diols, 6,6-*vic*-diol **1a** has a low acidity and reducibility ($pK_{a1}$ = 6.31; $\varepsilon$ = 0.53 V). 5,6-*vic*-diol **1b** and diol **1c** have a high acidity and reducibility ($pK_{a1}$ = –4.94, –3.72; $\varepsilon$ = –0.39 V, –0.29 V). Hence, structural unit **1b** and **1c** unlikely exist in their pristine forms in $C_{60}$ fullerenols prepared by strong alkali, oxidizing conditions, and **1a** likely exist. Instead, **1b** and **1c** will exist as the corresponding conjugate bases or oxidized products, *i.e.*, hemiacetals, isolated OH and epoxides. This structural prediction agrees with our NMR characterization using $^{13}C$-labeled $C_{60}$ fullerenols and is also consistent with the previous experimental results.

The structural model we developed and verified for $C_{60}$ fullerenols (Figure 6a) can consistently substantialize the electronic, IR and NMR spectroscopic properties observed for the fullerenols so far. Using the similar method, models for fullerenols with other molecular formula can also be built. Although the fullerenols have been studied for over twenty years and have been recently characterized to have potential medical applications,[34-36] little is known about the structures substantializing these properties. The model we present here thus provides a basis for studying molecular mechanisms underlying the many intriguing biomedical effects of the fullerenols. Especially, the model will be widely used in the future to take advantage of the various all-atom simulation approaches, which are indispensable to study the structure-activity relationships for fullerenols at atomistic levels.

## Methods

### Calculations

All geometry optimizations were performed using the B3LYP method in conjunction with the 6-31G(d,p) basis set in gas phase. Frequency analysis was done at the same level of theory for each structure to obtain the zero-point energy and entropy. Frequency calculations confirmed that each energy minimum had no imaginary frequencies and each transition state had one imaginary frequency. To consider the solvent effects, single-point energy calculations were done with the B3LYP/6-31+G(d,p) method and PCM solvent model on the basis of the optimized geometries. All calculations were performed using the GAUSSIAN 09 package.[37]

**Calculation of p$K_a$.** To calculate $pK_a$ for fullerenols (FOH), the following deprotonation reaction was considered,

$$FOH = FO^- + H^+, \quad \Delta G_1 \qquad (1)$$

where $\Delta G_1$ is change in Gibbs free energy for the deprotonation. Then, acid dissociation constant $pK_a$ can be obtained by

$$pK_{a,FOH} = \frac{\Delta G_1}{2.303RT} \qquad (2)$$

where $R$ is ideal gas constant, 8.314 $J{\cdot}K^{-1}{\cdot}mol^{-1}$, and $T$ is temperature. Because $\Delta G_1$ involves proton hydration energy, which is difficult to calculate directly, the following thermodynamic cycle was used. One considers the dissociation reaction of acetic acid (AcOH) Eq. 3 and the displacement reaction Eq. 4,

$$AcOH = AcO^- + H^+, \quad \Delta G_2 \qquad (3)$$

$$FOH + AcO^- = FO^- + AcOH, \quad \Delta G_3 \qquad (4)$$

where $pK_{a,\,AcOH}$ = 4.76, *i.e.*, experimental $pK_a$ of AcOH, and $\Delta G_1$ is the change in Gibbs free energy for reaction 4, which can be calculated by DFT.

Because Eq. 1 = Eq. 3 + Eq. 4, $\Delta G_1 = \Delta G_2 + \Delta G_3$. Bringing this relation into Eq. 2, one gets $pK_a$ for FOH

$$pK_{a,FOH} = \frac{\Delta G_2 + \Delta G_3}{2.303RT} = pK_{a,AcOH} + \frac{\Delta G_3}{2.303RT} \qquad (5)$$

**Calculation of $\varepsilon$.** To calculate redox potential $\varepsilon$ for fullerenols, the following reaction was considered,

$$FO + H^+ + e^- = FOH, \quad \Delta G_4 \qquad (6)$$

Then, $\varepsilon$ for redox couple FO/FOH can be calculated by

$$\varepsilon_{\mathrm{FO/FOH}} = -\frac{\Delta G_4}{nF} \quad (7)$$

where $n = 1$, *i.e.*, the number of transferred electrons in reaction 6, and $F$ is the Faraday constant, $9.65 \times 10^4$ J·V$^{-1}$·mol$^{-1}$. Similarly, to avoid the calculations of proton and electron hydration energies, the following thermodynamic cycle was employed.

$$\frac{1}{4}\mathrm{O_2} + \mathrm{H^+} + e^- = \frac{1}{2}\mathrm{H_2O}, \quad \Delta G_5 \quad (8)$$

$$\mathrm{FOH} + \frac{1}{4}\mathrm{O_2} = \mathrm{FO} + \frac{1}{2}\mathrm{H_2O}, \quad \Delta G_6 \quad (9)$$

Because Eq. 6 = Eq. 8 − Eq. 9, $\Delta G_4 = \Delta G_5 - \Delta G_6$. Bringing this relation into Eq. 7, one gets the redox potential for FO/FOH,

$$\varepsilon_{\mathrm{FO/FOH}} = -\frac{\Delta G_5 - \Delta G_6}{nF} = \varepsilon_{(\mathrm{O_2/H_2O})} + \frac{\Delta G_6}{nF} \quad (10)$$

where $\varepsilon_{\mathrm{O_2/H_2O}} = 0.815$, *i.e.*, the standard $\varepsilon$ value experimentally measured for $O_2/H_2O$, and $\Delta G_6$ is the change in Gibbs free energy for reaction 9, which can be calculated by DFT.

**Experiments**

We prepared $^{13}$C-labeled $C_{60}$ using the arc-discharge method and $^{13}$C-labeled graphite rods. As for the synthesis of $C_{60}$ fullerenols, we used a method similar to the previous ones.[10, 13] Briefly, a toluene solution of $^{13}$C-labeled $C_{60}$ (30 mg in 20 ml) was vigorously stirred with NaOH (1.5 g) powder and 0.5 mL of 50% TBAH (tetrabutylammonium hydroxide) at room temperature under air for 24 hours. The color of the toluene solution, originally, deep violet, turned colorless with a black brown sludge precipitated. After the reaction, a small amount of water was added. The organic phase was removed and the aqueous phase was filtered to remove a trace amount of water-insoluble residues. The filtrate was washed by 50 ml methanol, and then a brown precipitate appeared. After removal of methanol by vacuum-evaporation method, 5 ml water was added to the precipitate, which was then purified by Sephadex G-25 column chromatography (1×30 cm$^2$) with an eluent of neutralized water and vacuum freeze-drying to obtain 33.8 mg fullerenol powder. The fullerenol sample was then used to do IR and NMR characterization. The NMR experiments for the fullerenol sample were carried out on a Bruker Avance-300 spectrometer operating at 7 T. $^{13}$C magic-angle-spinning (mas) NMR spectra were acquired from samples spun in a rotor of diameter 4 mm at 10 kHz, applying aring sequence and a 30 s delay, and accumulating 2000 scans. $^1$H-$^{13}$C mas NMR spectra were recorded by the Hartmann-Hahn method, with 2 s delay and 7200 scans.

## Acknowledgements

This work was supported by the CAS Hundreds Elite Program, NSFC Project (21373226, 11005116), MOST 973 program (2012CB934001, 2011CB933400, 2011CB933101). We thank Prof. Gengmei Xing at Institute of High Energy Physics for discussion.

## Notes and references

[a] CAS Key Laboratory for Biomedical Effects of Nanomaterials and Nanosafety, Institute of High Energy Physics, Chinese Academy of Sciences, Beijing 100049, China

[b] Jiangxi Inorganic Membrane Materials Engineering Research Centre, College of Chemistry and Chemical Engineering, Jiangxi Normal University, Nanchang 330022, China

[c] National Laboratory of Solid State Microstructures, Department of Physics, Nanjing University, Nanjing 210093, China

† Z.W. and X.C. contributed equally.

Electronic Supplementary Information (ESI) available: [details of any supplementary information available should be included here]. See DOI: 10.1039/b000000x/

1. J. Grebowski, P. Kazmierska and A. Krokosz, *Biomed. Res. Int*, 2013.
2. F. Jiao, Y. Liu, Y. Qu, W. Li, G. Q. Zhou, C. C. Ge, Y. F. Li, B. Y. Sun and C. Y. Chen, *Carbon*, 2010, **48**, 2231-2243.
3. J. Meng, X. J. Liang, X. Y. Chen and Y. L. Zhao, *Integr. Biol.*, 2013, **5**, 43-47.
4. Z. Markovic and V. Trajkovic, *Biomaterials*, 2008, **29**, 3561-3573.
5. J. J. Yin, F. Lao, P. P. Fu, W. G. Wamer, Y. L. Zhao, P. C. Wang, Y. Qiu, B. Y. Sun, G. M. Xing, J. Q. Dong, X. J. Liang and C. Y. Chen, *Biomaterials*, 2009, **30**, 611-621.
6. Y. Liu, F. Jiao, Y. Qiu, W. Li, F. Lao, G. Q. Zhou, B. Y. Sun, G. M. Xing, J. Q. Dong, Y. L. Zhao, Z. F. Chai and C. Y. Chen, *Biomaterials*, 2009, **30**, 3934-3945.
7. X. J. Liang, H. Meng, Y. Z. Wang, H. Y. He, J. Meng, J. Lu, P. C. Wang, Y. L. Zhao, X. Y. Gao, B. Y. Sun, C. Y. Chen, G. M. Xing, D. W. Shen, M. M. Gottesman, Y. Wu, J. J. Yin and L. Jia, *P. Natl. Acad. Sci. USA.*, 2010, **107**, 7449-7454.
8. L. O. Husebo, B. Sitharaman, K. Furukawa, T. Kato and L. J. Wilson, *J. Am. Chem. Soc.*, 2004, **126**, 12055-12064.
9. K. Kokubo, K. Matsubayashi, H. Tategaki, H. Takada and T. Oshima, *ACS nano*, 2008, **2**, 327-333.
10. G. M. Xing, J. Zhang, Y. L. Zhao, J. Tang, B. Zhang, X. F. Gao, H. Yuan, L. Qu, W. B. Cao, Z. F. Chai, K. Ibrahim and R. Su, *J. Phys. Chem. B.*, 2004, **108**, 11473-11479.
11. L. Y. Chiang, J. B. Bhonsle, L. Y. Wang, S. F. Shu, T. M. Chang and J. R. Hwu, *Tetrahedron*, 1996, **52**, 4963-4972.
12. L. Y. Chiang, R. B. Upasani, J. W. Swirczewski and S. Soled, *J. Am. Chem. Soc.*, 1993, **115**, 5453-5457.
13. J. Li, M. Y. Zhang, B. Y. Sun, G. M. Xing, Y. Song, H. L. Guo, Y. A. Chang, Y. H. Ge and Y. L. Zhao, *Carbon*, 2012, **50**, 460-469.
14. A. Hirsch, *Fullerenes and Related Structures*, 1999
15. M. S. Meier and J. Kiegiel, *Org. Lett.*, 2001, **3**, 1717-1719.
16. T. F. Guarr, M. S. Meier, V. K. Vance and M. Clayton, *J. Am. Chem. Soc.*, 1993, **115**, 9862-9863.
17. C. C. Henderson and P. A. Cahill, *Science*, 1993, **259**, 1885-1887.
18. B. R. Weedon, R. C. Haddon, H. P. Spielmann and M. S. Meier, *J. Am. Chem. Soc.*, 1999, **121**, 335-340.
19. P. W. Atkins and J. De Paula, *Atkins' Physical chemistry*, Oxford University Press, Oxford; New York, 2006.
20. N. Matsuzawa, D. A. Dixon and T. Fukunaga, *J. Phys. Chem.*, 1992, **96**, 7594-7604.
21. A. Hirsch, *The chemistry of the fullerenes*, thieme, stuttgart, 1994.
22. S. H. Huang, Z. Xiao, F. D. Wang, L. B. Gan, X. Zhang, X. Q. Hu, S. W. Zhang, M. J. Lu, Q. Q. Pan and L. Xu, *J. Org. Chem.*, 2004, **69**, 2442-2453.



 

23. J. Y. Yao, D. Z. Yang, Z. Xiao, L. B. Gan and Z. M. Wang, *J. Org. Chem.*, 2009, **74**, 3528-3531.
24. D. V. Andreeva, O. V. Ratnikova, E. Y. Melenevskaya and A. V. Gribanov, *Int. J. Polym. Ana.l Ch.*, 2007, **12**, 105-113.
25. L. B. Casablanca, M. A. Shaibat, W. W. W. Cai, S. Park, R. Piner, R. S. Ruoff and Y. Ishii, *J. Am. Chem. Soc.*, 2010, **132**, 5672-5676.
26. W. W. Cai, R. D. Piner, F. J. Stadermann, S. Park, M. A. Shaibat, Y. Ishii, D. X. Yang, A. Velamakanni, S. J. An, M. Stoller, J. H. An, D. M. Chen and R. S. Ruoff, *Science*, 2008, **321**, 1815-1817.
27. S. Stankovich, D. A. Dikin, R. D. Piner, K. A. Kohlhaas, A. Kleinhammes, Y. Jia, Y. Wu, S. T. Nguyen and R. S. Ruoff, *Carbon*, 2007, **45**, 1558-1565.
28. Z. Xiao, J. Y. Yao, D. Z. Yang, F. D. Wang, S. H. Huang, L. B. Gan, Z. S. Jia, Z. P. Jiang, X. B. Yang, B. Zheng, G. Yuan, S. W. Zhang and Z. M. Wang, *J. Am. Chem. Soc.*, 2007, **129**, 16149-16162.
29. W. Gao, L. B. Alemany, L. J. Ci and P. M. Ajayan, *Nat. Chem.*, 2009, **1**, 403-408.
30. X. F. Gao, S. B. B. Zhang, Y. L. Zhao and S. Nagase, *Angew. Chem. Int. Ed.*, 2010, **49**, 6764-6767.
31. X. F. Gao, Y. L. Zhao, B. Liu, H. J. Xiang and S. B. B. Zhang, *Nanoscale*, 2012, **4**, 1171-1176.
32. X. F. Gao, Z. Q. Wei, V. Meunier, Y. Y. Sun and S. B. B. Zhang, *Chem. Phys. Lett.*, 2013, **555**, 1-6.
33. R. spin densitAnderson and A. R. Barron, *J. Am. Chem. Soc.*, 2005, **127**, 10458-10459.
34. P. Chaudhuri, A. Paraskar, S. Soni, R. A. Mashelkar and S. Sengupta, *ACS nano*, 2009, **3**, 2505-2514.
35. J. Q. Fan, G. Fang, F. Zeng, X. D. Wang and S. Z. Wu, *Small*, 2013, **9**, 613-621.
36. C. Y. Chen, G. M. Xing, J. X. Wang, Y. L. Zhao, B. Li, J. Tang, G. Jia, T. C. Wang, J. Sun, L. Xing, H. Yuan, Y. X. Gao, H. Meng, Z. Chen, F. Zhao, Z. F. Chai and X. H. Fang, *Nano Lett.*, 2005, **5**, 2050-2057.
37. M. J. Frisch, Gaussian, Inc., Wallingford CT, Revision A.1 ed, 2009.

Journal Name RSCPublishing

ARTICLE

# A Precision Structural Model for Fullerenols

Zhenzhen Wang,[a,b] Xueling Chang,[a] Zhanghui Lu,[b] Min Gu,[c] Yuliang Zhao,[*,a] and Xingfa Gao[*,a]

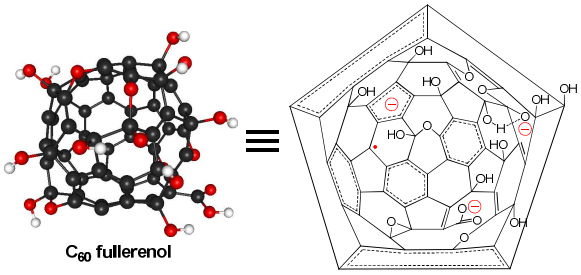


An explicit structural model was developed and verified for fullerenols.